Synthesis and Spectroscopic Characterization of Actinyl(VI) Tetrahalide Coordination Compounds Containing 2, 2'-Bipyridine.

Mikaela M. Pyrch, Jay M. Williams, Maguire W. Kasperski, Lindsey C. Applegate, and Tori Z. Forbes*

Department of Chemistry, University of Iowa, Iowa City, IA 52242, United States

*corresponding author: tori-forbes@uiowa.edu; 319-384-1320

Keywords: Uranyl, Neptunyl, Actinide complex, Raman Spectroscopy, Crystallography, Force Constants.

Abstract

A series of three new actinide tetrahalide coordination compounds containing 2,2'- bipyridinium (H_2bpy) have been synthesized by room temperature evaporation and characterized via single crystal X-ray diffraction, Raman spectroscopy, and infrared spectroscopy. The solid-state compounds (**Np1**, **U1**, and **U2**) contain the AnO_2^{2+} cation coordinated to four halide (chloride or bromide) atoms to form the anionic tetrahalide molecular unit $[AnO_2X_4]^{2-}$ (X = Cl, Br) charge balanced by the 2,2'-bipyridinium cation that engages in electrostatic interactions with the actinyl complex. **Np1** *$(N_2C_{10}H_{10})[NpO_2Cl_4]$* contains 2,2'- bipyridine in the *cis* conformation where both the nitrogen atoms are directed towards the $[NpO_2Cl_4]$ monomer. Within **U1** *$(N_2C_{10}H_9)[UO_2Cl_4]$*, the 2,2'- bipyridine is in a *trans* conformation, and found in the same conformation in the isomorphous structure **U2** *$(N_2C_{10}H_9)[UO_2Br_4]$*. The compounds were further characterized by vibrational spectroscopy with specific interest in the actinyl cation. Raman spectroscopy provided information on the actinyl symmetric stretch (ν_1) whereas IR spectroscopy is used to determine the location of the asymmetric stretch (ν_3). Spectral similarities are observed between the two isomorphous structures, but slight variations across the series of structures are found to be associated with bipyridine bands in the various conformations. Additional analysis of these vibrational features in **U1** and **U2** provided information on the actinyl force constants, allowing insight into the relative uranyl bond strength that was compared to similar tetrahalide compounds.

Highlights

- Synthesis of three new actinide halide complexes using slow evaporation.
- Characterization of the complexes via single crystal X-ray diffraction, Raman spectroscopy, and IR spectroscopy.
- Protonation of 2,2'- bipyridine introduces structural changes resulting in increased supramolecular assembly sites.
- Calculation of force constants for the uranyl cation provides information on relative bond strength.

1. Introduction

A substantial issue associated with the use of nuclear reactors for power generation is the formation of hazardous, radioactive waste products.[1] The nuclear fuel cycle within the United States can be considered an open cycle as there are limited efforts in fuel reprocessing and the waste is destined for long term storage in a geologic repository[1-3]. Only one storage site in the United states (Waste Isolation Pilot Plant (WIPP) in New Mexico) is currently operational and accepts transuranic solid wastes.[4] This repository is positioned within a 2,000-foot-thick salt bed that was created during repeated evaporation of an ancient Permian sea.[5-7] While the waste is securely stored within the site, there is concern that long-term storage could lead to the release of radioactive materials into the environment. Given the high salt concentration, any water present in the environment will be a brine with high concentration of halide anions (up to 175,000 ppm Cl^-).[4, 6-11] Therefore, it is vitally important to be able to predict actinide speciation and behavior within high ionic strength solutions to develop accurate transport modeling.[10]

Within ionic brines, actinide speciation is driven by high oxidation state complexes where the actinyl moiety ($AnO_2^{+/2+}$) is a dominant bonding motif.[12-13] Uranium (U) typically exists in the hexavalent oxidation state under these conditions, while neptunium (Np) can exist as several possible valence states (IV, V, or VI).[14-15] Wang *et al.* has suggested that Np(V) is the stable form in solution within high ionic strength solutions, but redox of the metal cation leads to the formation and identification of Np(VI) in the solid state.[14, 16] In either the penta- or hexavalent states, both U and Np will form strong bonds to two oxygen atoms, creating the nearly linear dioxo $[An(V/VI)O_2]^{+/2+}$ cation.[13] Additional bonding occurs to four, five, or six equatorial atoms from ligands to create a square, pentagonal, and hexagonal bipyramidal geometry about the metal center.[17-18] In high salt and high acid concentrations the speciation of the uranyl cation is known,

with the $[UO_2X_a(H_2O)_{4-a}]^{2-a}$ (X = Cl^-, Br^-; a = 1-4) species occurring when the ionic strength ranges from 300 to 3000 molal, but less is known regarding specific Np(V/VI) speciation in these conditions.[19]

Structural and chemical characterization of uranyl halide coordination compounds can provide important information regarding bond strength and reactivity.[20-21] Solid compounds that contain uranyl (UO_2^{2+}) halide species are more commonly found in the literature because ^{238}U is a naturally occurring radionuclide with a long half-life (4.5 x 10^9 years). [7-9] Neptunium halide coordination complexes are less reported due to additional hazards when working with the most stable isotope (^{237}Np $t_{1/2}$ = 2.14 x 10^6 years). A major initiative within the Forbes research group is aimed at understanding the impact of the actinyl cation on chemical properties of solid-state compounds. By partnering spectroscopy with diffraction techniques, we hope to provide direct correlation of structure-property relationships within actinyl materials. Herein, we describe the structural and spectral features for actinyl tetrahalide coordination compounds (**Np1** *($N_2C_{10}H_{10}$)[Np(VI)O_2Cl_4]*, **U1** *($N_2C_{10}H_9$)[U(VI)O_2Cl_4]*, and **U2** *($N_2C_{10}H_9$)[U(VI)O_2Br_4]*). The ligand 2,2'-byridine (2,2'-bipy) was chosen as a crystallization agent because of its versatility within the crystalline lattice.[22] For example, the 2,2'bipyridine ligand can coordinate directly to metal centers, exist as a neutral lattice molecule (bipy), or form cationic species as singly protonated (Hbipy) or doubly protonated (H_2bipy) moieties.[23] The compounds reported herein crystallize with the Hbipy and H_2bipy cations and demonstrate that subtle differences in the protonation state of the bipyridine ligand influence crystalline packing and related spectral signals.

2. Experimental

2.1 Synthesis.

Caution: *These experiments require the use of ^{238}U ($t_{1/2}$ = 3.8 x 10^9 years)) and ^{237}Np ($t_{1/2}$ = 2.14 x 10^6 years). Both of these actinide elements are alpha-emitters and only should be handled by trained personnel with appropriate facilities to handle these radioactive materials.*

All experiments utilize the 2,2'- bipyridine *($N_2C_{10}H_8$)* (bipy) ligand, which was purchased from Sigma Aldrich and used as received without additional purification. Hexavalent uranium was purchased from International Bio-analytical Industries as uranyl acetate dihydrate *$[UO_2(C_2O_2H_3)_2]\cdot 2H_2O$* and used as received. Solid NpO_2 was purchased from the Isotope Program at Oakridge National Laboratory, dissolved in 6 M HNO_3, and subjected to ozonolysis to promote oxidation and dissolution of the solid. After eight hours of ozonolysis, the mixed Np(V/VI) solution was reduced to Np(V) using $NaNO_2$, precipitated using saturated NaOH, and the gray-green solid was rinsed with ultrapure H_2O three times. This solid Np(V) phase was dissolved in 1.0 M HCl for the experimental stock solution. The concentration of the Np stock solution was determined using a Packard Tri-Carb Liquid Scintillation Counter and the oxidation state of the stock solution was confirmed with Raman spectroscopy.

Np1 *$(N_2C_{10}H_{10})[Np(VI)O_2Cl_4]$* was synthesized by adding 300 µL of a 65 mM Np(V) stock solution and 400 µL of a 100 mM 2,2'- bipyridine solution into a glass vial. The vial was allowed to evaporate uncapped for three days. After this time, 150 µL was removed and placed into a crystallization well. After 8 hours of slow evaporation, yellow plate-like crystals of **Np1** precipitated from the solution. Given the highly radioactive nature of the material, quantitative yields could not be determined for the Np solid phases, but qualitatively the yields are reported as moderate.

U1 *$(N_2C_{10}H_9)[U(VI)O_2Cl_4]$* was formed from 0.313g of uranyl acetate dihydrate dissolved in 2.0 mL of methanol in a 30mL glass beaker, followed by addition of 2.0 mL of concentrated

(12N) HCl and the 2,2'-bipy ligand (2.0 mL of 0.4M H_2O stock) This solution was mixed with a magnetic stir bar and heated at 110 °C until 3.0 mL of yellow solution remained in the beaker. Long yellow rods of **U1** appeared on the bottom of the beaker within 4 hours of slow evaporation with yields of 80-90% based upon U.

U2 *$(N_2C_{10}H_9)[U(VI)O_2Br_4]$* was crystallized from the dissolution of 0.0253g of uranyl acetate dihydrate in 5.0 mL of methanol with the addition of 2.0 mL of 47% by weight HBr. This solution was stirred and heated at 110 °C until the total volume of the solution was 3mL. After cooling, 2.0 mL of 0.4M 2,2'-bipy was added and allowed to slowly evaporate at room temperature. Crystalline yellow rods of **U2** appeared after 4 hours of evaporation with percent yields of 80-90% based on U.

2.2 Single-Crystal X-Ray Diffraction

Single crystals of **Np1**, **U1**, and **U2** were separated from the mother liquor and mounted on a MiTeGen MicroMount using NVH immersion oil (Cargille Labs). All frames were collected on a Bruker D8 Quest single crystal X-ray diffractometer equipped with a microfocus beam (Mo Kα; λ = 0.71073 Å). Matrix, ω, and φ scans were collected using the Bruker APEX3 software package[24]. Total peak intensities were corrected for (Lorentz, polarization, background effects, and absorption). The initial structure solution was determined by intrinsic phasing methods and refined on the basis of F^2 for all unique data using the SHELXTL version 5 programs.[25] The actinide atoms (U and Np) were located by direct methods, additional atoms (C, O, N, Cl, Br) were found and modeled from the difference Fourier maps. Hydrogen atoms were found in the Fourier map and refined isotropically for all three structures. Select crystallographic parameters are available in Table 1 while choice bond distances and angles can be found in Tables S1-S3. The

crystallographic information files can be found on the Cambridge Structural Database by requesting numbers 1976228-1976230.

Table 1. Select crystallographic parameters for compounds **Np1**, **U1**, and **U2**.

	Np1	**U1**	**U2**
Empirical formula	$NpC_{20}H_{18}N_4O_2Cl_4$	$UC_{10}H_{10}N_2O_2Cl_4$	$UC_{10}H_{10}N_2O_2Br_4$
Formula weight	362.59	570.03	747.87
Space group	*P*-1	$P2_1/n$	$P2_1/n$
a (Å)	8.9380(11)	8.9096(3)	9.069(2)
*b (*Å)	9.3693(10)	12.0572(4)	12.288(3)
*c (*Å)	9.4764(11)	14.5287(5)	14.992(4)
α (°)	119.165(4)	90	90
β (°)	92.054(4)	94.5930(10)	93.940(9)
γ (°)	115.604(4)	90	90
V ($Å^3$)	593.53(12)	1555.73(9)	1666.8(7)
Z	1	4	4
ρ (g/cm^3)	2.029	2.434	2.980
μ (mm^{-1})	4.852	11.117	19.325
F(000)	343	1040	1328
θ range for data collection (°)	2.661 to 26.421°	2.593 to 26.372°	2.550 to 26.165°
Limiting indices	-11≤h≤11	-11≤h≤11	-11≤h≤11
	-11≤k≤11	-15≤k≤15	-15≤k≤15
	-11≤1≤11	-18≤l≤18	-18≤l≤18
Reflections collected / unique	36316/2429	40913/ 3181	42405/ 3309
R_{int}	0.0304	0.0455	0.0645
Data / restraints / parameters	2429 / 0 / 178	3181 / 0 / 215	3309 / 0 / 215
GOF on F^2	1.164	1.093	1.050
Final R indices	R_1 = 0.0111	R_1 = 0.0223	R_1 = 0.0224
[I>2σ(I)]	wR_2 = 0.0275	wR_2= 0.0455	wR_2= 0.0448
R indices (all data)	R_1 = 0.0111	R_1 = 0.0395	R_1 = 0.0359
	wR_2 = 0.0275	wR_2 = 0.0505	wR_2 = 0.0485
Largest diff. peak and hole ($e.Å^{-3}$)	0.215 and -0.521	0.679 and -1.072	0.896 and -1.233

2.3 Vibrational Spectroscopy

To collect solid state Raman spectra, crystals of compounds **Np1**, **U1**, and **U2** were isolated from the mother liquor and placed on a glass slide with a small amount of NVH immersion oil. Solid-state spectra of the bipy ligand were also collected as a standard for spectral analysis. All spectra were acquired on a SnRI High-Resolution Sierra 2.0 Raman spectrometer equipped with 785 nm laser energy and 2048 pixels TE-cooled CCD. Laser power was set to the maximum output value of 15 mW, giving the highest achievable spectral resolution of 2 cm^{-1}. Each sample (**Np1**, **U1**, and **U2**) was irradiated for separate integration times of 60, 15 and 5 seconds, respectively, and automatically reiterated five times in Multi-Acquisition mode. The average of the five scans acquired for a sample is reported as the final spectrum. Bands of interest were analyzed in the OriginPro 9.1.0 (OriginLab, Northampton, MA) 64-bit software package by a background subtraction followed by peak fitting using Lorentzian functions.[26] This provides a full width half max (FWHM) of each signal and more accurate values associated with the peak centroid. Infrared spectra of 2,2'-bipy, **U1** and **U2** were collected from 400 to 4000cm^{-1} with a Nicolet Nexus 760 FTIR spectrometer, by pressing a pellet containing solid KBr and a small quantity of crystalline sample.

3 Results and Discussions

3.1 Structural Descriptions

Np1 crystallizes in the centrosymmetric triclinic space group *P*-1 with a single $[Np^{VI}O_2Cl_4]^{2-}$ moiety and one Hbipy molecule in the asymmetric unit (Fig. 1). The $[Np^{VI}O_2Cl_4]^{2-}$ anion contains Np=O bonds at a distance of 1.7525(13)Å and O=Np=O angle of 180.0(9)º. Two unique equatorial Np-Cl bonds are present and create the overall square bipyramidal coordination

geometry by reflection through the inversion center. The Np-Cl bond distances are 2.6364(6) and 2.6719(5) Å. One unique 2,2' bipyridine is crystallized in the *cis* form with the N atoms directed towards the chlorine atoms of the $[Np^{VI}O_2Cl_4]$ in the equatorial plane. A single nitrogen (N2) is protonated and the hydrogen could be observed within the difference Fourier map after refinement of the other atoms in the structure.

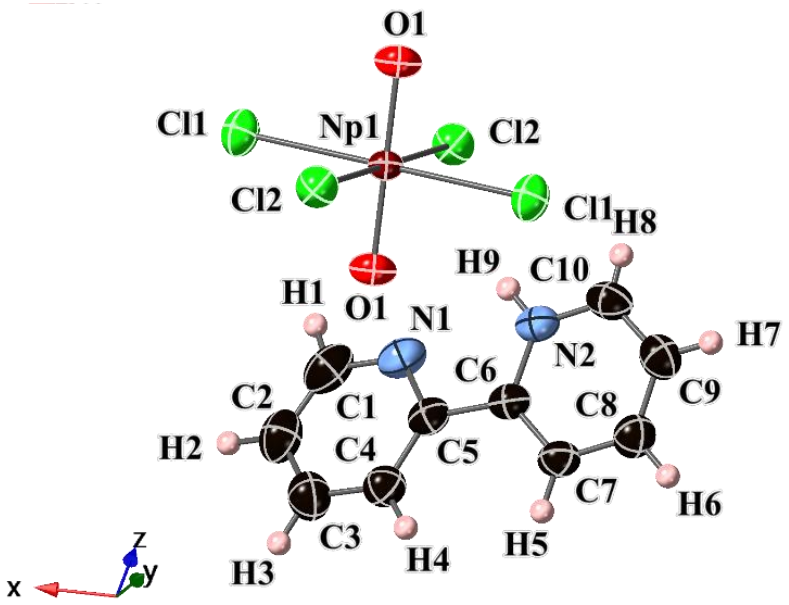

Figure 1. Thermal ellipsoids at 50% probability level of **Np1,** with the Np cation depicted as a maroon ellipsoid. The O, Cl, C, and N atoms are represented by red, green, black, and blue ellipsoids, respectively. The H atoms have been included as pink spheres.

The extended lattice of **Np1** assembles primarily through hydrogen bonding interactions that stem from the Hbipy molecule. Three total H bonds are observed originating from the Hbipy ligand and are tabulated in Table 2. The first interactions are C8-H6···O1, with O1 being the oxo group on the $[Np^{VI}O_2Cl_4]^{2-}$ complex and a donor to acceptor distance (d(D-A)) of 3.177 Å. The remaining two hydrogen bonding interactions involve the Cl atoms on the $[Np^{VI}O_2Cl_4]^{2-}$ complex (N2-H9···Cl2 and C10-H8···Cl1) with D-A distances of 3.274 and 3.318 Å, respectively. A

potential halogen-halogen interaction is noted at 4.078 Å, but the distance is significantly beyond the sum of the van der Waals radii of 3.5 Å. Thus, we did not consider the Cl1···Cl1* a true interaction. The extended figure of **Np1** can be found in the Supplementary information (SI Figure 1 and 2).

Table 2. The interactions present within **Np1**, **U1**, and **U2**, that assemble the individual units into the extended structure. The donor(D), acceptor(A), and overall distances are included. For interactions involving hydrogen, the donor is the parent atom to which the hydrogen is directly bound.

Interaction	Donor	Acceptor	d(D-h)	d(H-A)	d(D-A)
Np1					
C8-H6···O1	C8	O1	0.95(3)	2.526	3.177
N2-H9···Cl2	N2	Cl2	0.83(3)	2.533	3.274
C10-H8···Cl1	C10	Cl1	0.79(3)	3.220	3.318
Cl1···Cl1*	Cl1	Cl1*	NA	NA	4.078
U1					
C10-H4···O1	C10	O1	0.94(4)	2.442	3.343
C7-H1···O1	C7	O1	0.84(4)	2.664	3.470
N1-H5···Cl1	N1	Cl1	0.79(4)	2.436	3.212
C4-H6···Cl1	C4	Cl1	0.86(3)	2.896	3.492
C9-H3···Cl2	C9	Cl2	1.00(4)	2.773	3.684
C2-H8···O2	C2	O2	0.84(4)	2.487	3.244
O1···Cl3	Cl3	O1	NA	NA	3.377
U2					
C2-H7···O1	C2	O1	0.92(5)	2.440	3.261
C10-H2···O2	C10	O2	0.88(5)	2.623	3.476
N2-H1···Br4	N2	Br4	0.80(4)	2.617	3.385
C4-H10···Br4	C4	Br4	0.87(4)	2.958	3.593
N1-H9···Br2	N1	Br2	0.74(4)	2.619	3.325
C7-H5···O2	C7	O2	0.89(4)	2.694	3.540
C8-H4···Br4	C8	Br4	0.95(5)	2.881	3.608
C9-H3···Br3	C9	Br3	1.03(5)	2.914	3.849
O2···Br2	Br2	O2	NA	NA	3.429

Compound **U1** crystallized in the $P2_1/n$ space group and contains two $[U^{VI}O_2Cl_4]^{2-}$ coordination complexes within the asymmetric unit (Fig.2). The uranyl U=O bond lengths are

1.768(2) and 1.752(2) Å with a reported O=U=O angle of 180°. For both U(VI) species, coordination about the metal center is completed by four chloride atoms in the equatorial plane, with U-Cl_{eq} bond distances ranging between 2.6302(9) and 2.7054(9) Å. A H_2bipy molecule is found in the second coordination sphere in a *trans* antiperiplanar conformation.

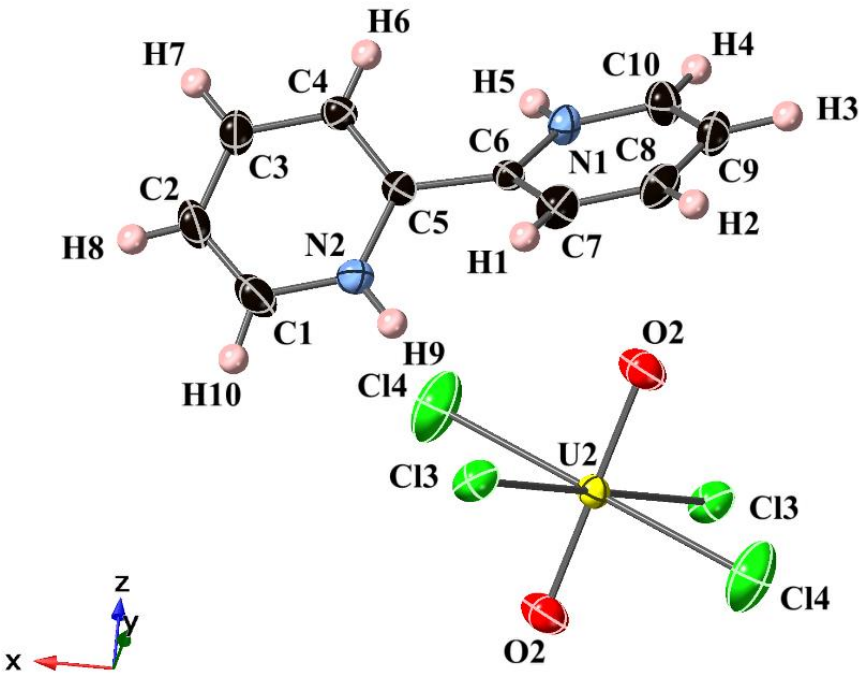

Figure 2. Thermal ellipsoids at 50% probability level representation for **U1**. The U, O, C, Cl, and N atoms are represented by yellow, red, black, green, and blue spheres, respectively. The H atoms have been included as pink spheres.

Assembly of the **U1** lattice occurs primarily through hydrogen bonding interactions originating from the protonated H_2bipy ligand, compiled in Table 2. There are three hydrogen bonds between the H_2bipy donor where a halogen acts as the acceptor (N1-H5···Cl1,C4-H6···Cl1, and C9-H3···Cl2). Three additional interactions occur between the H_2bipy ligand and the oxo group associated with the uranyl cation (C2-H8···O2, C7-H1···O1, and C10-H4···O1). The average bond

distances for the hydrogen-halogen interactions and the hydrogen-oxo contacts measured from the donor to acceptor are 3.46 and 3.35 Å, respectively. One potential O1···Cl3 contact occurs at 3.377 Å, which is just beyond the sum of the van der Waals radii for oxygen and chlorine (3.35 Å). The extended figure of **U1** is available in the Supplementary information (SI Figure 3).

Compound **U2** crystallizes in the $P2_1/n$ space group, shown in Figure 3, and is isomorphous to the **U1** material. The sole difference is the identity of the halogen bound to the U(VI) cation, with Cl^- anions present in **U1** and Br^- anions in **U2**. Two $[U^{VI}O_2Br_4]^{2-}$ units are present in the asymmetric unit with U=O bond lengths of 1.770(3) and 1.755(3)Å both with an O=U=O angle of 180º. The square bipyramidal coordination geometry around the U(1) and U(2) cations are completed by four bromide atoms in the equatorial plane, with U-Br_{eq} bond distances ranging between 2.7858(8) and 2.8488(6)Å. The Hbipy ligand is also observed in a *trans* antiperiplanar conformation to create the isomorphous **U1** structure.

Hydrogen bonding is again the driving force in the crystallization of the extended lattice for **U2** (SI Figure 4). Five total hydrogen bonds occur from the H_2bipy molecule with a halogen atom serving as the acceptor (N2-H1···Br4, C4-H10···Br4, N1-H9···Br2, C8-H4···Br4, and C9-H3···Br3) shown in Table 2.. The donor to acceptor distance (d(D-A)) for the hydrogen to halogen bonds range from 3.325-3.849 Å. There are three hydrogen interactions with the oxo groups associated with the uranyl cation C7-H5···O2, C2-H7···O1, and C2-H7···O1 with an average distance of 3.425 Å. There is one potential halogen-oxygen interaction occurring between O2···Br2 at a distance of 3.429 Å but it lies outside of the ideal sum of the van der Waals radii for oxygen and bromine at 3.37Å.

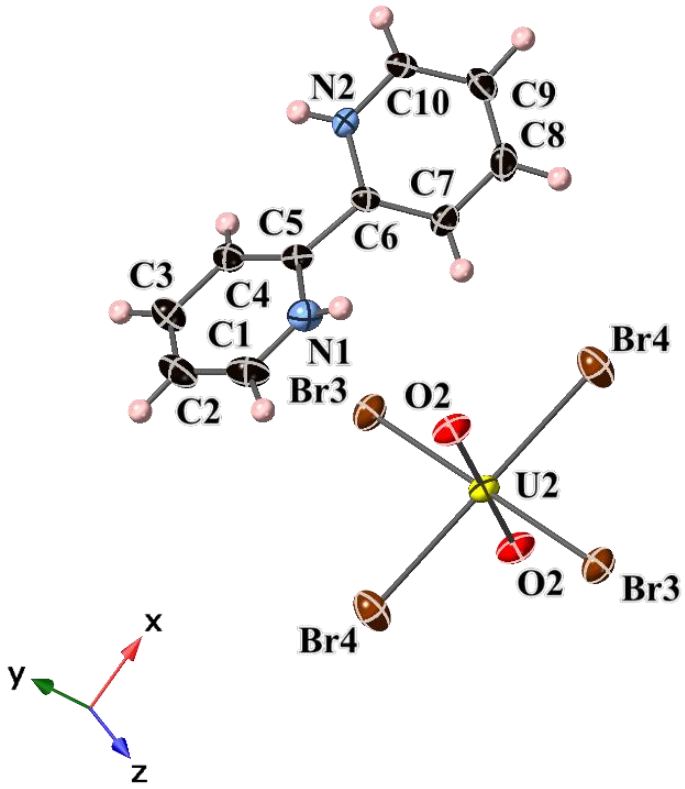

Figure 3. Thermal ellipsoids at 50% probability level for **U2.** The U, O, C, N, and Br atoms are represented by yellow, red, black, and blue, and brown ellipsoids, respectively, while the H atoms are depicted as pink spheres.

Studies by Danis *et al.,* Schanaars and Wilson, and others have resulted in the isolation of the actinyl(VI) tetrahalide $[U^{VI}O_2Cl_4]^{2-}$ complex in a variety of chemical systems, spanning from pyridyl ligands to crown ethers, all resulting in a diverse assembly of the $[An^{VI}O_2Cl_4]^{2-}$ into supramolecular motifs.[27-31] Fewer structures are reported for tetrabromide species, yet commonly are found to be isostructural to their chloride analogs.[11] Within the Np(VI) system, Cornet *et al*., Basile *et al*., Pyrch *et al.,* and others have all reported compounds that contain the $[NpO_2Cl_4]^{2-}$ anion.[32-37] Only one $[Np(V)O_2Cl_4]^{3-}$ coordination complex has been reported[38] and Cornet *et al.* noted that the $[Np(VI)O_2Cl_4]^{2-}$ anion seemed to be surprising stable in protic solvents based upon the ease of crystallization for this tetrachloro species.[33]

The role of the counterion is an important factor in the crystallization of the actinyl tetrahalide solid-state phases and two bipy isomers are observed within the compounds reported herein that is dependent on the protonation state. For the *cis* confirmation, the N atoms are located on the same side of the bipy ligand, whereas rotation of one heterocycle about the central C-C bond results in the *trans* isomer (Fig. 4). Howard performed *ab initio* modeling of the neutral conformers and found that the *trans* conformation is more stable in the gas phase, but the energetics of interconversion to the *cis* isomer is only 6 kJ/mol.[39] With monoprotonation, Howard determined that the *cis* conformer was now thermodynamically favored and the energy for conversion to the trans isomer was +14 kJ/mol.[39] Therefore, the *cis* isomer is the most common configuration for monoprotonated species, whereas the *trans* conformer is observed with protonation of both N atoms.[26] The role of pH and solvent in the protonation of the bipy molecule and the formation of specific conformers was confirmed experimentally by Nakamoto.[40]

Conditions for crystallization within the U(VI) and Np(VI) system may have impacted the resulting protonation of the bipy species. With slow evaporation techniques, the total volume of the mother liquor is reduced, which leads to higher concentrations of the HCl or HBr. The **Np1** compound resulted from an initially lower acidic concentrations, which favors the monoprotonated state of Hbipy cation and the *cis*-conformation (Fig. 4a). The uranyl compounds, **U1** and **U2**, were also formed using highly acidic media (conc HCl, or 47% by weight HBr), so the experimental conditions lent themselves to crystallizing the doubly-protonated *trans*-conformation of H_2bipy cation (Fig. 4b). [41]

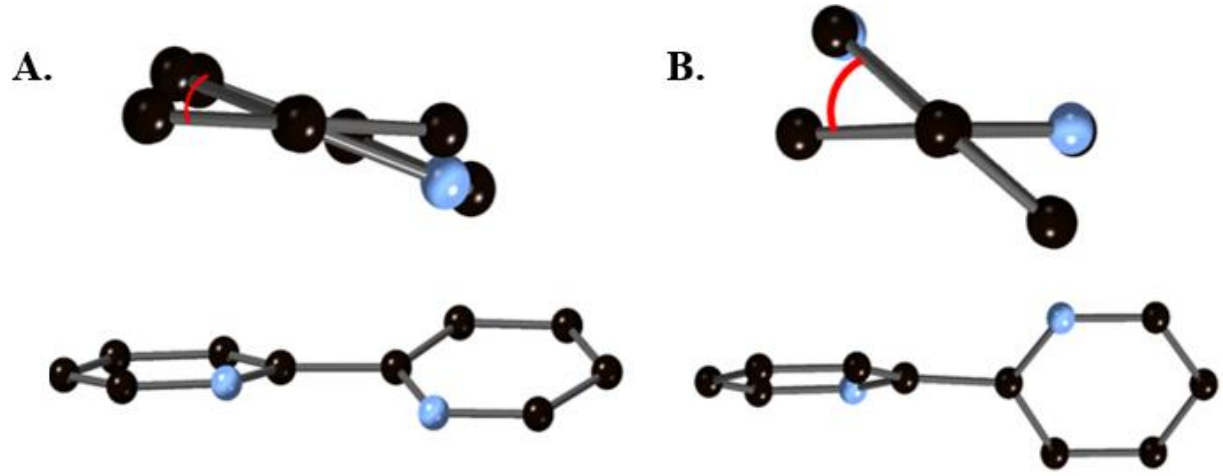

Figure 4. The two crystallized modes of 2,2' -bipyridine in a *cis* planar conformation found for **Np1** (**A**) and *trans* antiperiplanar conformation found in **U1** and **U2 (B)**, with N and C atoms represented as light blue and black spheres, respectively.

Changes in protonation also result in variations in the molecular geometry of the bipy cation, which impacts the intermolecular interactions within the extended lattice. We observed χ values of 17° and 143° for the *cis* and *trans* conformers, respectively. This agrees well with the *ab initio* models by Howard, which determined χ values of 0 and 153° for the *cis* and *trans* isomers of the bipy cation, respectively.[39] The change in the molecular geometry is likely due to repulsion from the H atoms associated with the N-H bond that then results in torsion about the C-C linkage. [42] This in turn can influence the extended hydrogen bonding network with the crystalline material and this phenomenon is observed within the structural characteristics of **Np1**, **U1**, and **U2**. Both **U1** and **U2** have increased hydrogen bonding between the protonated amine of the H_2bipy ligand and neighboring halogen and/or oxo groups of the $[U^{VI}O_2X_4]^{2-}$ complex. Subtle differences are observed between **U1** and **U2** that are based upon the identity of the halogen, as bromine is more polarizable than chlorine.[20] **Np1** has fewer overall interactions stemming from the bipyridine then **U1** and **U2**, and we attribute this to the monoprotonation of the Hbipy cation in comparison to the doubly protonated H_2bipy cation in **U1** and **U2.**

Calestani *et al*. reported the formation of the $(Hbipy)_2[UO_2Cl_4]$ solid in 1987 that was then reanalyzed by Marsh *et al.* in 1988. [43-44] The original study suggested a triclinic *P*1 space group with a = 9.375(2) Å, b = 9.487(2) Å, c = 8.870(2) Å, alpha = 91.8(1) °, beta = 115.0(1) °, and gamma = 119.0(1)°, but Marsh *et al*. determined that a higher space group was appropriate (*P*-1) . Within the crystalline lattice of this phase, there is a single $[U^{VI}O_2Cl_4]$ unit with Hbipy ligands located within the interstitial regions in a planar *cis* conformation. The bond lengths for U=O was 1.768(7) Å and average U-Cl distance being 2.675 Å. In our two uranyl structures, **U1** and **U2**, the bipy unit is in an antiperiplanar *trans* conformation (as highlighted in Figure 4) and both nitrogen atoms are protonated. **Np1** crystalizes with the Hbipy in a similar fashion to the uranyl structure reported by Marsh to form an isomorphic pairing.

The importance of the type and specific bonding within the actinyl tetrahalide coordination compounds have been previously noted to influence the bond strength of the actinyl bond and the vibrational features. A clear example of the impact of the counter ion is within the $[NpO_2Cl_4]^{2-}$ system was reported by Bjorklund *et al*.[32] This study evaluated the impact of alkali metal cations on the neptunyl bond and found that the Li^+ cation, with its high charge density, engaged with the oxo group and resulted in a significant red shift of the neptunyl stretch observed within the Raman spectrum. Within the uranyl system, Ohwada investigated the vibrational signatures of uranyl halides with a variety of counter cations, reporting that lattice waters in crystalline uranyl chloride systems can influence the vibrational signals of the tetrachloride anion, and focused on assigning infrared peaks taking into account the effects of metal cations on the tetrachloride species by estimation of force constants. [12-14] Further efforts by Schnaars and Wilson observed that polymorphic variations also resulted in shifts of the vibrational bands within the spectra.[29] We

will further explore the spectral features and force constants associated with the Hbipy and H_2bipy actinyl tetrahalide compounds in the next section.

3.3 Vibrational Spectroscopy

Symmetric (ν_1) and asymmetric (ν_3) stretches for both the uranyl and neptunyl cation are typically observed as intense bands in the vibrational spectra and will shift depending on the coordination to the actinyl cation. The actinyl cation typically possess the $D_{\infty h}$ point group symmetry, leading to a Raman active symmetric stretch.[13, 45] The asymmetric stretch and bending modes are both present in the infrared spectra, but the degenerate bending features are observed at low energies and are relatively weak compared to the stretching modes. Identity of the ligands that bind to the actinyl cation through the equatorial plane are important because additional sigma donation or electrostatic interaction with the Np(V), Np(VI), or U(VI) metal center can cause a red shift of the ν_1 band to lower wavenumbers. Typically, the pentaaqua complex serves as the reference point to understand the impact on the actinyl bond due to minimal sigma donation of the ligated water molecules. Therefore the band shift is given as referenced to the peak centroid of the $[An(H_2O)_5]^{2+}$ band occurring at 870, and 854 cm^{-1} for the ν_1 symmetric stretch and at 959, and 969 cm^{-1} for the ν_3 symmetric stretch associated with the U(VI), and Np(VI) species, respectively.[46-48] We will be focusing on the spectral window of interest for these two stretching features (Raman = 750-900 cm^{-1}; IR = 700-1000 cm^{-1}) and a table summarizing the bands in the Raman spectra for each complex and solid bipy starting material can be found in the supporting information in Table S4. Unfitted Raman spectra for **Np1**, **U1**, and **U2** can be found in the supplemental information (SI Figure 5-7) while fittings of the Raman spectra for **Np1**, **U1**, and **U2** can be seen in figure 5 with a table of the peak centroids and FWHM for each fitted band is found

in SI table 5. As a note, due to the higher radioactivity of the **Np1** compound, only the Raman spectrum could be collected for this compound.

Multiple bands are observed the Raman spectra of the actinyl tetrahalide compounds and these features were assigned to the actinyl symmetric stretch and bands associated with Hbipy and H_2bipy cations. For **Np1** compound, we observe the ν_1 symmetric stretch at 814 cm^{-1}, while this feature occurred at 825 and 826 cm^{-1} for the **U1** and **U2** phases, respectively. In all cases, the symmetric stretching mode is red shifted from the pentaaqua reference point, suggesting additional sigma donation or influenced by the electrostatics of the halide anion as previously suggested by Vallet *et al*.[49] The ν_1 band for the **Np1** compound is red shifted by 11-12cm^{-1} in comparison to is uranyl analogs, which is typically caused by to changes in bond length and electronic structure of the actinide cation.[13, 21] The symmetric stretch (ν_1) for uranyl tetrachloride ranges from 820-840 cm^{-1} and the related bromide species can be observed in a similar region (815-835 cm^{-1}).[27, 45] Spectral features at approximately 760 and 790 cm^{-1} are observed in all three compounds and can be assigned to the bipy ligand.[40] Additional bands are found at 772, 848, and 865 cm^{-1} for **U1** and **U2**, which correspond to activation of the H_2bpy within the *trans* antiperiplanar conformation. Spectral features observed between 980-1175cm^{-1} are related to ring breathing modes, ring stretching bands, and C-H in plane deformations of the Hbipy and H_2bipy cation.[27-29]

Five major bands are observed within the infrared spectra for the uranyl tetrahalide coordination complexes and are similarly positioned at approximately 750, 790, 860, 904, and 931 cm^{-1}. IR spectra for **U1**, **U2** and bipy are reported in supplementary information Figures 8-10, and summarization of the peak centroids for each are reported in SI table 5. The features at approximately 750, 790, and 860 cm^{-1} can be assigned to the H_2bipy cation, but we could not initially determine if the ν_3 uranyl asymmetric stretch corresponded to the band at 904 or 931 cm^{-}

[1]. This issue highlights the difficulties in assigning the uranyl asymmetric stretch within the FTIR spectra of hybrid materials because it occurs within the fingerprint region and can potentially overlap with modes associated with organic molecules.[50-53] Previous spectral characterization of uranyl tetrahalide compounds indicate that the asymmetric stretch of the $[UO_2Cl_4]^{2-}$ species occurs from 904 to 923 cm^{-1} and the range narrows for the analogous tetrabromide species (904-913 cm^{-1}).[29, 32, 52, 54-55] This suggests that the band at 904 cm^{-1} can be considered the uranyl asymmetric stretch for both the **U1** and **U2** compounds. However, previous spectral analysis of the neutral bipy ligand also suggests that the band at 904 cm^{-1} may be assigned to a ring breathing mode, so the identity of the peak was not certain.[53]

To provide insight into the spectral analysis, we utilized the linear regression developed specifically for tetrachloride coordination compounds that was previously published in Lu *et al.* (SI Fig.11).[45] In this case, the ν_1 and ν_3 were plotted and a linear regression was performed with an R^2 of 0.86. The linear relationship ($y = 0.9674x + 107.04$) was then used to predict the position of the ν_3 band based upon our ν_1 experimental value. With a symmetric stretch present at 826 cm^{-1}, the ν_3 band was then predicted to occur at 905 cm^{-1}, which is within one cm^{-1} of the experimental value. Combining our understanding of the previously reported compounds with our linear regression allows confidence in assigning the ν_3 band for **U1** and **U2** compounds as 904 cm^{-1}.

Assignment of both the ν_1 and ν_3 uranyl stretching bands for the **U1** and **U2** compounds provides additional information on bond strength because it allows us to calculate the force constants associated with the uranyl cation, as shown by Lu *et.al*, Schnaars and Wilson, and Carter *et.al*.[29, 45, 56-57] Additional information regarding the calculation of force constants from spectral data and the calculated values for the characterized uranyl tetrahalide species are provided in the SI, including the final equations for k_1 and k_{12} (SI Eq. 1 and 2). The force constant (k_1) value for

U1 and **U2** are 6.60 and 6.61 mdyn/Å, respectively. This value is within the range (6.53-6.85 mdyn/Å) for known tetrahalide complexes but is lower than the average value of 6.71(8) mdyn/Å). The interaction force constant (k_{12}) is -0.19 and -0.18 mdyn/Å for **U1** and **U2**, respectively, and again fits within the range of previously reported compounds.

Closer analysis of the $[UO_2X_4]^{2-}$ X = Cl^-, Br^- literature (SI Table 6) also indicated that that our calculated force constant values for **U2** and **U2** agree well with that of $[PPh_4]_2UO_2Cl_4$ ($P2_1/c$) (k_1 = 6.58 mdyn/Å, k_{12} = -0.20 mdyn/Å) that was previously published by Schnaars and Wilson.[29] This work demonstrated that the exact bonding and arrangement of the $[UO_2X_4]^{2-}$ X = Cl^-, Br^- complexes and charge balancing cations within the crystalline lattice could impact the band positions and force constants for polymorphs. Schnaars and Wilson observed that the uranyl stretching modes of the related $[PPh_4]_2UO_2Cl_4$ ($P\bar{1}$) phase were blue shifted (ν_1 = 838 cm^{-1}; ν_3 = 919 cm^{-1}) compared to the monoclinic form and the force constant was higher (k_1 = 6.81 mdyn/Å). **U1** and **U2** both crystallize in the monoclinic $P2_1/n$ space group and display similar weak H-bonding networks as observed in the $[PPh_4]_2UO_2Cl_4$ ($P2_1/c$) phase. Therefore, this result further support the hypothesis that the crystalline packing associated intermolecular interaction can influence the overall vibrational spectra.

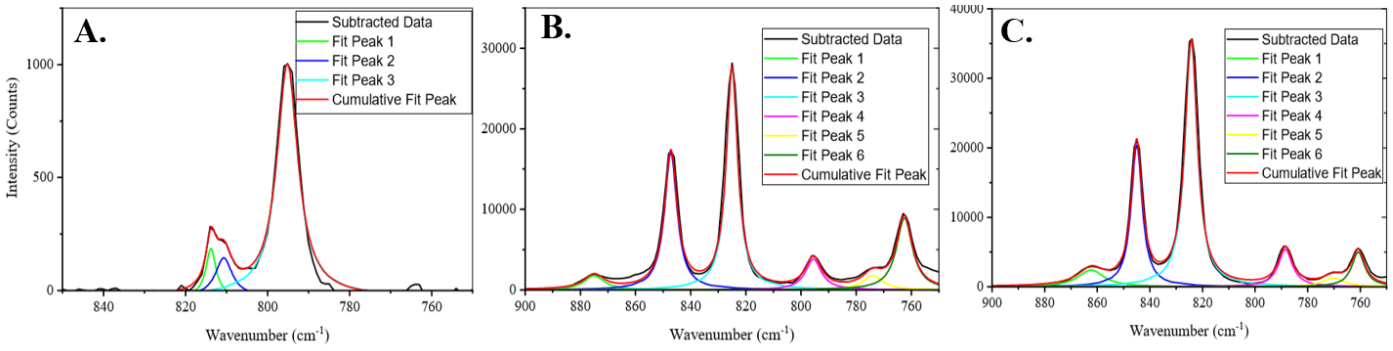

Figure 5: Fitted Raman spectra for (A) **Np1**, (B) **U1**, and (C) **U2**.

4 Conclusions

Synthetic conditions that resulted in the crystallization of two new uranyl halide coordination complex (**U1** and **U2**) and one new neptunyl chloride phase (**Np1**) were reported and structural characterization of the material was performed via single crystal X-ray diffraction. All three compounds contained the $[An(VI)O_2X_4]^{2-}$ (An = U, Np; X = Cl, Br) moiety and crystallized through electrostatic and H-bonding interactions with either the Hbipy or H_2bipy cation. **U1** and **U2** compounds are isostructural with a torqued H_2bipy molecule coordinating via hydrogen – halide interactions. This contrasts with the **Np1** phase in which the Hbipy ligand remains planar. These compounds were further characterized by vibrational spectroscopy and both the symmetric and asymmetric stretching modes for the actinyl cations were red-shifted compared to the pentaaqua reference point. Evaluating the relationship between the ν_1 and ν_3 bands for previously reported uranyl tetrahalide compounds allowed us to confirm the position of the ν_3 band for **U1** and **U2**. Position of the uranyl stretching bands also provided information on the uranyl force constants and could be compared to previously reported uranyl tetrachloride species that crystallized through weak hydrogen bonding interactions and within a monoclinic lattice.

Acknowledgements

The authors would like to thank Dr. Ed Gillian at the University of Iowa for the use of his FTIR. We would like to acknowledge the Department of Energy Early Career Award (DE-SC0013980) for supporting this work.

Supporting Information Available

References

1. Macfarlane, A. M.; Miller, M., Nuclear Energy and Uranium Resources. *Elements* **2007,** *3* (3), 185-192.
2. Ewing, R. C., Nuclear Fuel Cycle: Environmental Impact. *MRS Bulletin* **2008,** *33* (4), 338-340.
3. Ewing, R. C., The Nuclear Fuel Cycle: A Role for Mineralogy and Geochemistry. *Elements* **2006,** *2* (6), 331-334.
4. Lambert, S. J., Geochemistry of the waste isolation pilot plant (WIPP) site, southestern New Mexico, U.S.A. *Applied Geochemistry* **1992,** *7* (6), 513-531.
5. Engle, M. A.; Reyes, F. R.; Varonka, M. S.; Orem, W. H.; Ma, L.; Ianno, A. J.; Schell, T. M.; Xu, P.; Carroll, K. C., Geochemistry of formation waters from the Wolfcamp and "Cline" shales: Insights into brine origin, reservoir connectivity, and fluid flow in the Permian Basin, USA. *Chemical Geology* **2016,** *425*, 76-92.
6. Saller, A. H.; Stueber, A. M., Evolution of formation waters in the Permian Basin, United States: Late Permian evaporated seawater to Neogene meteoric water. *AAPG Bulletin* **2018,** *102* (3), 401-428.
7. Stueber, A. M.; Saller, A. H.; Ishida, H., Origin, migration, and mixing of brines in the Permian basin: geochemical evidence from the eastern Central Basin Platform, Texas. *AAPG Bulletin* **1998,** *82* (9), 1652-1672.
8. Brush, L. H.; Grbic-Galic, D.; Reed, D. T.; Tong, X.; Vreeland, R. H.; Westerman, R. E., Preliminary Results of Laboratory Studies of Repository Chemistry for the Waste Isolation Pilot Plant. *MRS Proceedings* **1990,** *212*, 893.
9. Pederson, L. R.; Clark, D. E.; Hodges, F. N.; McVpy, G. L.; Rai, D., The Expected Environment for Waste Packages in a Salt Repository. *MRS Proceedings* **1983,** *26*, 417.
10. Lucchini, J. F.; Borkowski, M.; Richmann Michael, K.; Reed Donald, T., Uranium(VI) solubility in carbonate-free WIPP brine. In *Radiochimica Acta International journal for chemical aspects of nuclear science and technology*, 2013; Vol. 101, p 391.
11. Roedder, E.; Belkin, H. E., Thermal Gradient Migration of Fluid Inclusions in Single Crystals of Salt from the Waste Isolation Pilot Plant Site (WIPP). In *Scientific Basis for Nuclear Waste Management*, Northrup, C. J. M., Ed. Springer US: Boston, MA, 1980; pp 453-464.
12. Clark, A. E.; Samuels, A.; Wisuri, K.; Landstrom, S.; Saul, T., Sensitivity of Solvation Environment to Oxidation State and Position in the Early Actinide Period. *Inorg Chem* **2015,** *54* (13), 6216-25.
13. Denning, R. G., Electronic structure and bonding in actinyl ions and their analogs. *J Phys Chem A* **2007,** *111* (20), 4125-43.
14. Antonio, M. R.; Soderholm, L.; Williams, C. W.; Blaudeau, J. P.; Bursten, B. E., Neptunium redox speciation. *Radiochim. Acta* **2001,** *89*, 17.
15. Kihara, S.; Yoshida, Z.; Aoyagi, H.; Maeda, K.; Shirai, O.; Kitatsuji, Y.; Yoshida, Y., A Critical Evaluation of the Redox Properties of Uranium, Neptunium and Plutonium Ions in Acidic Aqueous Solutions. In *Pure and Applied Chemistry*, 1999; Vol. 71, p 1771.
16. Wang, S.; Alekseev, E. V.; Ling, J.; Skanthakumar, S.; Soderholm, L.; Depmeier, W.; Albrecht-Schmitt, T. E., Neptunium Diverges Sharply from Uranium and Plutonium in Crystalline Borate Matrixes: Insights into the Complex Behavior of the Early Actinides Relevant to Nuclear Waste Storage. *Angewandte Chemie International Edition* **2010,** *49* (7), 1263-1266.
17. Knope, K. E.; Soderholm, L., Solution and Solid-State Structural Chemistry of Actinide Hydrates and Their Hydrolysis and Condensation Products. *Chemical Reviews* **2013,** *113* (2), 944-994.
18. Andrews, M. B.; Cahill, C. L., Uranyl Bearing Hybrid Materials: Synthesis, Speciation, and Solid-State Structures. *Chemical Reviews* **2013,** *113* (2), 1121-1136.
19. Nguyen-Trung, C.; Begun, G. M.; Palmer, D. A., *Inorg. Chem.* **1992,** *31*, 5280.
20. Su, J.; Dau, P. D.; Qiu, Y.-H.; Liu, H.-T.; Xu, C.-F.; Huang, D.-L.; Wang, L.-S.; Li, J., Probing the Electronic Structure and Chemical Bonding in Tricoordinate Uranyl Complexes UO2X3– (X = F, Cl, Br,

I): Competition between Coulomb Repulsion and U–X Bonding. *Inorganic Chemistry* **2013,** *52* (11), 6617-6626.
21. Hayton, T. W.; Wu, G., Exploring the effects of reduction or Lewis acid coordination on the U=O bond of the uranyl moiety. *Inorg Chem* **2009,** *48* (7), 3065-72.
22. Kaes, C.; Katz, A.; Hosseini, M. W., Bipyridine: The Most Widely Used Ligand. A Review of Molecules Comprising at Least Two 2,2‘-Bipyridine Units. *Chemical Reviews* **2000,** *100* (10), 3553-3590.
23. Moissette, A.; Batonneau, Y.; Brémard, C., Conformation and Protonation of 2,2‘-Bipyridine and 4,4‘-Bipyridine in Acidic Aqueous Media and Acidic ZSM-5 Zeolites: A Raman Scattering Study. *Journal of the American Chemical Society* **2001,** *123* (49), 12325-12334.
24. Sheldrick, G. M. *APEX3*, Bruker AXS: Madison, WI, 2015.
25. Sheldrick, G. M., *Acta Crystallographica Section A: Foundations of Crystallography* **2008,** *64*, 112-122.
26. *Origin(Pro)*, 2019b; OriginLab Corporation.
27. Danis, J. A.; Lin, M. R.; Scott, B. L.; Eichhorn, B. W.; Runde, W. H., Coordination Trends in Alkali Metal Crown Ether Uranyl Halide Complexes: The Series [A(Crown)]2[UO2X4] Where A = Li, Na, K and X = Cl, Br. *Inorganic Chemistry* **2001,** *40* (14), 3389-3394.
28. Liu, G.; Deifel, N. P.; Cahill, C. L.; Zhurov, V. V.; Pinkerton, A. A., Charge Transfer Vibronic Transitions in Uranyl Tetrachloride Compounds. *The Journal of Physical Chemistry A* **2012,** *116* (2), 855-864.
29. Schnaars, D. D.; Wilson, R. E., Structural and Vibrational Properties of U(VI)O2Cl42- and Pu(VI)O2Cl42- Complexes. *Inorganic Chemistry* **2013,** *52* (24), 14138-14147.
30. Deifel, N. P.; Cahill, C. L., The uranyl tetrachloride anion as a tecton in the assembly of U(VI) hybrid materials. *CrystEngComm* **2009,** *11* (12), 2739-2744.
31. Deifel, N. P.; Cahill, C. L., Supramolecular chemistry with uranyl tetrahalide ([UO2X4]2−) anions. *Comptes Rendus Chimie* **2010,** *13* (6), 747-754.
32. Bjorklund, J. L.; Pyrch, M. M.; Basile, M. C.; Mason, S. E.; Forbes, T. Z., Actinyl-cation interactions: experimental and theoretical assessment of [Np(vi)O2Cl4]2− and [U(vi)O2Cl4]2− systems. *Dalton Transactions* **2019,** *48* (24), 8861-8871.
33. Cornet, S. M.; Redmond, M. P.; Collison, D.; Sharrad, C. A.; Helliwell, M.; Warren, J., The unusual stability of [NpO2Cl4]2−: Synthesis and characterisation of [NpO2(DPPMO2)2Cl]2[NpO2Cl4] and [Ph3PNH2]2[NpO2Cl4]. *Comptes Rendus Chimie* **2010,** *13* (6), 832-838.
34. Pyrch, M. M.; Williams, J. M.; Forbes, T. Z., Exploring crown-ether functionalization on the stabilization of hexavalent neptunium. *Chemical Communications* **2019,** *55* (63), 9319-9322.
35. Clark, D. L.; Conradson, S. D.; Donohoe, R. J.; Gordon, P. L.; Keogh, D. W.; Palmer, P. D.; Scott, B. L.; Tait, C. D., Chemical Speciation of Neptunium(VI) under Strongly Alkaline Conditions. Structure, Composition, and Oxo Ligand Exchange. *Inorganic Chemistry* **2013,** *52* (7), 3547-3555.
36. Surbella, R. G.; Ducati, L. C.; Pellegrini, K. L.; McNamara, B. K.; Autschbach, J.; Schwantes, J. M.; Cahill, C. L., Transuranic Hybrid Materials: Crystallographic and Computational Metrics of Supramolecular Assembly. *Journal of the American Chemical Society* **2017,** *139* (31), 10843-10855.
37. Wilkerson, M.; Dewey, H.; Gordon, P.; Scott, B., Synthesis and structure of ditetrabutylammonium tetrachlorodioxoneptunium(VI). *J Chem Crystallogr* **2004,** *34* (11), 807-811.
38. Payne, M. K.; Pyrch, M. M.; Jubinsky, M.; Basile, M. C.; Forbes, T. Z., Impacts of oxo interactions within actinyl metal organic materials: highlight on thermal expansion behaviour. *Chemical Communications* **2018,** *54* (77), 10828-10831.
39. Howard, S. T., Conformers, Energetics, and Basicity of 2,2‘-Bipyridine. *Journal of the American Chemical Society* **1996,** *118* (42), 10269-10274.
40. Nakamoto, K., ULTRAVIOLET SPECTRA AND STRUCTURES OF 2,2'-BIPYRIDINE AND 2,2',2″-TERPYRIDINE IN AQUEOUS SOLUTION1. *The Journal of Physical Chemistry* **1960,** *64* (10), 1420-1425.
41. Barker, D. J.; Summers, L. A.; Cooney, R. P., Conformations of 2,2′-bipyridine in acidic media. *Journal of Molecular Structure* **1987,** *159* (3), 249-254.

42. Grummt, U.-W.; Erhardt, S., Torsional profiles of protonated and metal-coordinated 2,2′-bipyridine. *Journal of Molecular Structure: THEOCHEM* **2004,** *685*, 133-137.
43. Marsh, R. E., Crystal structure of di-(2,2′-pyridylpyridinium)tetrachlorodioxouranate(VI). *Journal of Crystallographic and Spectroscopic Research* **1988,** *18* (2), 219-222.
44. Calestani, G.; Montenero, A.; Bettinelli, M.; Tellini, L.; Ingletto, G., Crystal and molecular structure of di-(2,2′-pyridylpyridinium)tetrachlorodioxouranate (VI). *Journal of Crystallographic and Spectroscopic Research* **1987,** *17* (2), 251-258.
45. Lu, G.; Haes, A. J.; Forbes, T. Z., Detection and identification of solids, surfaces, and solutions of uranium using vibrational spectroscopy. *Coordination Chemistry Reviews* **2018,** *374*, 314-344.
46. Madic, C.; Begun, G. M.; Hobart, D. E.; Hahn, R. L., Raman spectroscopy of neptunyl and plutonyl in aqueous solutions: hydrolysis of Np(VI) and Pu(VI) and disproportionation of Pu(V). *Inorganica Chimica Acta* **1984,** *94* (1), 100-102.
47. Basile, L. J.; Sullivan, J. C.; Ferraro, J. R.; LaBonville, P., The Raman Scattering of Uranyl and Transuranium V, VI, and VII Ions. *Appl. Spectrosc.* **1974,** *28* (2), 142-145.
48. Gál, M.; Goggin, P. L.; Mink, J., Mid-, far-infrared and raman spectra of uranyl complexes in aqueous solutions. *Journal of Molecular Structure* **1984,** *114*, 459-462.
49. Vallet, V.; Wahlgren, U.; Grenthe, I., Probing the Nature of Chemical Bonding in Uranyl(VI) Complexes with Quantum Chemical Methods. *The Journal of Physical Chemistry A* **2012,** *116* (50), 12373-12380.
50. de Groot, J.; Gojdas, K.; Unruh, D. K.; Forbes, T. Z., Use of Charge-Assisted Hydrogen Bonding in the Supramolecular Assembly of Hybrid Uranyl Materials. *Crystal Growth & Design* **2014,** *14* (3), 1357-1365.
51. Ohwada, K., Vibrational assignments of crystalline waters in some uranyl halide complexes. *Journal of Inorganic and Nuclear Chemistry* **1979,** *41* (8), 1145-1147.
52. Schnaars, D. D.; Wilson, R. E., Lattice Solvent and Crystal Phase Effects on the Vibrational Spectra of UO2Cl42–. *Inorganic Chemistry* **2014,** *53* (20), 11036-11045.
53. Castellucci, E.; Angeloni, L.; Neto, N.; Sbrana, G., IR and Raman spectra of A 2,2′-bipyridine single crystal: internal modes. *Chemical Physics* **1979,** *43* (3), 365-373.
54. Qu, F.; Zhu, Q.-Q.; Liu, C.-L., Crystallization in Ionic Liquids: Synthesis, Properties, and Polymorphs of Uranyl Salts. *Crystal Growth & Design* **2014,** *14* (12), 6421-6432.
55. Bullock, J. I.; Parrett, F. W., The low frequency infrared and Raman spectroscopic studies of some uranyl complexes: the deformation frequency of the uranyl ion. *Canadian Journal of Chemistry* **1970,** *48* (19), 3095-3097.
56. Carter, K. P.; Kalaj, M.; Surbella III, R. G.; Ducati, L. C.; Autschbach, J.; Cahill, C. L., Engaging the Terminal: Promoting Halogen Bonding Interactions with Uranyl Oxo Atoms. *Chemistry – A European Journal* **2017,** *23* (61), 15355-15369.
57. Kalaj, M.; Carter, K. P.; Cahill, C. L., Isolating Equatorial and Oxo Based Influences on Uranyl Vibrational Spectroscopy in a Family of Hybrid Materials Featuring Halogen Bonding Interactions with Uranyl Oxo Atoms. *European Journal of Inorganic Chemistry* **2017,** *2017* (40), 4702-4713.